# Sphere extreme AO control scheme: final performance assessment and on sky validation of the first auto-tuned LQG based operational system (Orale)

C. Petit, J.F. Sauvage, T. Fusco, A. Sevin, M. Suarez, A. Costille, A. Vigan, C. Soenke, D. Perret, S. Rochat, et al.

# SPHERE eXtreme AO control scheme: final performance assessment and on sky validation of the first auto-tuned LQG based operational system

C. Petit*[a], J.-F. Sauvage[a], T. Fusco[a,b], A. Sevin[c], M. Suarez[d], A. Costille[b], A. Vigan[b], C. Soenke[d], D. Perret[c], S. Rochat[f], A. Baruffolo[e], B. Salasnich[e] , J.-L. Beuzit[f], K. Dohlen[b], D. Mouillet[f], P. Puget[f], F. Wildi[g], M. Kasper[d], J.-M. Conan[a], C. Kulcsár[h], H.-F. Raynaud[h]

[a] ONERA, The French Aerospace Lab, Châtillon, France; [b]Laboratoire d'Astrophysique de Marseille, France; [c]Observatoire de Paris, France; [d]ESO, Garching, Germany; [e]INAF, Italia, [f]Institut de Planétologie et d'Astrophysique de Grenoble, France; [g]University of Genève, Switzerland; [h]Institut d'Optique Graduate School, France

## ABSTRACT

The SPHERE (Spectro-Polarimetry High-contrast Exoplanet Research) instrument is an ESO project aiming at the direct detection of extra-solar planets. SPHERE has been successfully integrated and tested in Europe end 2013 and has been re-integrated at Paranal in Chile early 2014 for a first light at the beginning of May. The heart of the SPHERE instrument is its eXtreme Adaptive Optics (XAO) SAXO (SPHERE AO for eXoplanet Observation) subsystem that provides extremely high correction of turbulence and very accurate stabilization of images for coronagraphic purpose. However, SAXO, as well as the overall instrument, must also provide constant operability overnights, ensuring robustness and autonomy. An original control scheme has been developed to satisfy this challenging dichotomy. It includes in particular both an Optimized Modal Gain Integrator (OMGI) to control the Deformable Mirror (DM) and a Linear Quadratic Gaussian (LQG) control law to manage the tip-tilt (TT) mirror. LQG allows optimal estimation and prediction of turbulent angle of arrival but also of possible vibrations. A specific and unprecedented control scheme has been developed to continuously adapt and optimize LQG control ensuring a constant match to turbulence and vibrations characteristics. SPHERE is thus the first operational system implementing LQG, with automatic adjustment of its models.

SAXO has demonstrated performance beyond expectations during tests in Europe, in spite of internal limitations. Very first results have been obtained on sky last May. We thus come back to SAXO control scheme, focusing in particular on the LQG based TT control and the various upgrades that have been made to enhance further the performance ensuring constant operability and robustness. We finally propose performance assessment based on in lab performance and first on sky results and discuss further possible improvements.

**Keywords:** Adaptive Optics, High Contrast Imaging, Control

## 1. INTRODUCTION

The SPHERE instrument [1] has successfully passed Preliminary Acceptance in Europe (PAE) end 2013, before shipping to Chile. After a few weeks of re-integration and check, SPHERE has seen its first light beginning of May 2014, providing for its first runs very promising results [2]. SPHERE eXtreme Adaptive Optics, SAXO, has demonstrated operability and encouraging preliminary performance [3, 4], though tuning and optimization are still required as well as full understanding of input signals and residuals. In this article we focus on the specific (Image) Tip-Tilt Mirror (ITTM) control. Indeed, SAXO is the first operational AO system designed to implement Linear Quadratic Gaussian (LQG) control, as well as automatic on-sky tuning. This implementation of LQG relies only on a fixed model structure, parameters being directly identified from on-sky data. Though the LQG control scheme has been already demonstrated in lab [5, 6] and on sky with the CANARY pathfinder [7], none of these validations relied on fully automated tuning.

* cyril.petit@onera.fr; phone 33 146734754

We propose here a brief analysis of PAE results concerning ITTM control, and demonstrate its performance in the integration phase. We discuss the current limitations and possible upgrades. We also propose first analysis of on-sky data and results. In particular, we analyze the Tip-Tilt input signal as observed on-sky, which proves to be atypical and induces an unexpected loss of performance [3] irrespective of the control solution. We then discuss performance of LQG compared to integrator, coupled to the on-line identification procedure defined for SPHERE [8].

We first recall SAXO global control architecture and features in Section 2. We briefly summarize the various control loops specificities and performance, but quickly focus on ITTM control through LQG in Section 3. We then recall the LQG control scheme and its interaction with the identification procedure. Section 4 is dedicated to in lab validation and performance assessment of the ITTM control law during PAE. On-sky results are discussed in Section 5.

## 2. SAXO CONTROL SCHEME OVERVIEW

SAXO control architecture has been elaborated from SAXO top level requirements and discussed in [9]. We just summarize here the SAXO control main features.

### 2.1 Global architecture

SAXO system global design has led to the specification, design and realization of the following components:

- A 40x40 visible Shack-Hartmann (VIS-WFS) measuring the atmospheric and common path phase perturbations, the position of the telescope pupil. This is an EMCCD technology component provided by ESO. It is associated to a focal plane pinhole for aliasing suppression [10].
- A high spatial (41x41 actuators) and temporal (1.2kHz) frequencies Deformable Mirror (DM) to correct for phase perturbations but the tip-tilt. This Stacked Array Mirror has been provided by CILAS.
- A fast (1.2Khz) image TT Mirror (ITTM) located in a pupil plane for image motion correction. This component has been taylor-made by Observatoire de Paris.
- A slow (1Hz) pupil TT Mirror (PTTM) close to the entrance focal plane to correct for pupil shifts. This is a PI component.
- A slow (1Hz) infra-red tip-tilt sensor (IR-WFS) on the scientific channel measuring the differential tip-tilt between the common and imaging paths,
- A slow (1Hz) differential image TT Plate (DTTP) located in a pupil plane (in the VIS-WFS path) to correct for differential tip-tilt between the imaging and VIS-WFS paths,
- A Real-Time Calculator (RTC): the SPARTA platform [11], built by ESO.

The SAXO system is thus composed of four loops plus one on-line calibration:

- Main AO loops (1.2 kHz): correct for atmospheric, telescope and common path defects. It comprises both high order modes compensation by the DM loop and low order modes (angle of arrival) compensation by the Image Tip-Tilt Mirror (ITTM) loop.
- The Differential TT Plate (DTTP) loop for fine centering on coronagraph mask (correction of differential tip-tilt between VIS and NIR channel).
- The Pupil TT Mirror (PTTM) loop for pupil shift correction (telescope and instrument).
- Non Common Path Aberrations (NCPA) pre-compensation which will lead to the reduction of persistent speckles [12].

This architecture is summarized in Figure 1. To be complete, one shall add to this diagram additional features:

- Tip-Tilt and Focus offload, which is a slow rate (0.016Hz) feed-forward servo-control involving RTC and telescope control,

- Derotation control, which involves Telescope control and SPHERE derotator but also RTC (see pupil loop control),
- on-line operations such as gain optimization or LQG model identification, ensured by the SPARTA cluster
- interaction between RTC and the INstrument Software (INS).

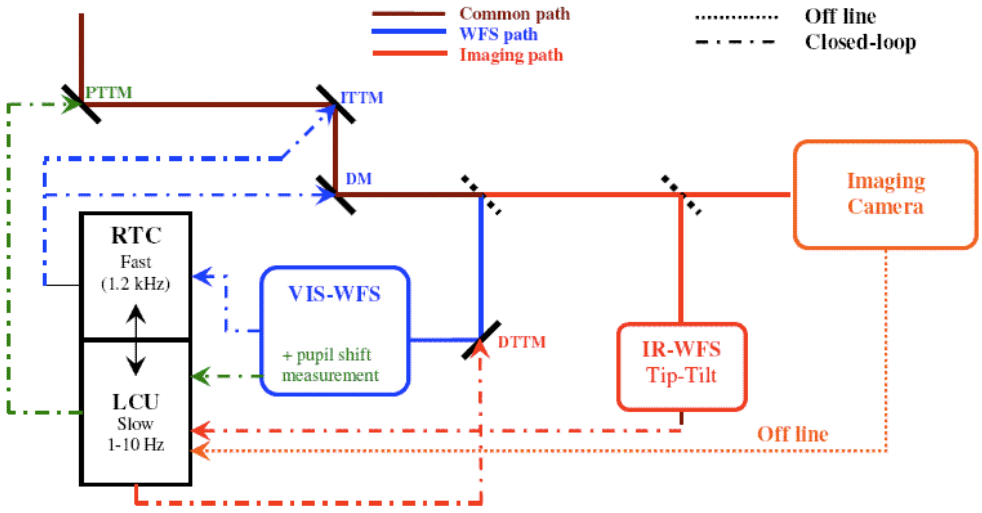


Figure 1: Schematic representation of SAXO loops.

We now discuss the various control loops of SAXO and their specific features.

### 2.2 Control loops overview

We only propose a short discussion of the various control loops main features and global performance as obtained at PAE and on-sky. Still, more details on the various control loops and their performance shall be provided in the future in a dedicated paper. Some aspects on global performance may be found in [3].

#### 2.2.1 Secondary loops

The secondary loops include the pupil motion correction and the differential Tip-Tilt correction. These two control loops are rather straightforward and implement basic integral controller, with fixed gain. Gain may be adapted to observation conditions. These loops have been successfully validated in term of control law, bandwidth, delay (2 frame delay) and performance [3].

Still, some key features require particular attention. First, the pupil motion control must account for pupil derotation. In the pupil stabilized mode, derotation is ensured by the derotator situated between the pupil Tip-Tilt mirror and the AO WFS. As a consequence, the interaction matrix (or equivalently the control matrix) of the PTTM must be derotated on-line according to the derotator position. Second, the Differential Tip-Tilt loop works by introduction of an additional Tip-Tilt in the AO WFSing arm through the DTTP. Decoupling with the main AO TT loop is basically ensured by the strongly different sampling frequencies. The DTTP loop is essential for the fine centering of the star on the coronagraph. Most of the PAE and on sky tests dedicated to DTTP have been focused on precise centering and repeatability of DTTP loop demonstrating a performance well within specifications [3].

#### 2.2.2 HO loop control

The High Order control loop shall control the DM up to 1.2 KHz. System Analysis has shown that a simple Optimized Modal Gain Integrator (OMGI) is enough to ensure the performance. Still, on-line optimisation of modal gains is

required. It is performed every 30 seconds using method derived from [13] and similar to NAOS one. In addition, correct choice of the modal basis must be considered dealing with a 1377 actuator DM [9]. A Karhunen Loève basis has been chosen. Finally, saturation handling, through antiwind-up is required, particularly considering the faint star and the poor conditions observations use cases considered [12]. It is associated to Garbage Collection (GC) to control and nullify the filtered modes that may evolve in open-loop. Practical integration of DM has also shown that it suffers from dead or badly responding actuators, as well as edge actuators, hardly visible in the pupil. All dead or badly responding actuators are declared inactive and all the control process (basis definition) is performed irrespective of these actuators. As for edge actuators, they are control using static slaving, that is computation of offset voltages on edge actuators as linear combination of their closest active neighbor. They are not controlled during closed-loop.

PAE and on-sky tests have validated this control loop, functionality of OMGI and significant gain brought by anti wind-up and GC though these aspects are not discussed here.

#### 2.2.3 Tip Tilt loop

The ITTM shall correct for turbulent angle of arrival, as well as possible and time evolving vibrations. To fulfill this requirement, a Linear Quadratic Gaussian control solution has been chosen following results obtained in lab demonstrating the ability of this control approach to compensate simultaneously turbulence and vibrations [5]. However, a dedicated identification procedure was needed to allow on-line auto-tuning of the LQG control solution to turbulence conditions and time evolving vibrations. Solution is based on [8], with additional improvements have been proposed. In addition, as for DM, the identification procedure and ITTM control have been constrained by the ITTM hardware limitations.

The next sections discuss the ITTM control loops features and performance.

#### 2.2.4 Control loops separation

As HODM can generate measurements similar to ITTM (in practice angle of arrival), decoupling of the control laws is necessary. The solution that has been proposed [9] relies on least-square projection and reduction of the HODM control space to the orthogonal of the HODM space which measurement is parallel to ITTM action on WFS. In practice this means removing two HODM modes, and separating any real-time WFS measurement (noted $s$ in the sequel) into a parallel $s_{//}$ and orthogonal $s_{\perp}$ component, the parallel one is fed to the ITTM LQG control, the orthogonal one to the HODM control loop.

## 3. SAXO ITTM CONTROL SCHEME

We propose in this section a compact description of the ITTM control scheme, as it basically relies on an LQG control approach already presented by the authors in the past, though in other context or partially.

### 3.1 Linear Quadratic Gaussian control

In the following we make the usual assumptions and notations:

- We consider a discrete-time control [14]
- ITTM is linear and its interaction matrix is noted $D_{ITTM}$
- Control voltages sent to ITTM at instant *n* are noted $u_n^{ITTM}$

- LQG control is performed in an orthonormal basis noted $(s_1, s_2)$ deduced from the measurements associated to ITTM actuation (interaction matrix) by simple re-orthonormalisation. Matrix $P$ performs the projection of any WFS measurement $s$ onto this basis so that $s_{//} = Ps$ and $s_{\perp} = s - s_{//}$
- We assume the system to have a 2 frame delay, which has been verified at 1.2KHz frame rate (2.14 precisely [9], delay issue discussed in the following section).

Contrary to usual application of LQG in AO where turbulent phase is estimated (for instance on a Zernike basis), here control (and thus estimation and prediction) are performed in the ITTM space. This is motivated by the absence of global estimation and reconstruction of turbulence, as higher order modes are controlled through OMGI on HODM space, and the ambition of optimal control of only the angle of arrival which matches the ITTM action. It has the advantage of simplifying the control equations.

We consider in the framework of SAXO that angle of arrival is composed of:

- 2 independent axis,
- a turbulent component per axis,
- up to 10 vibrations per axis, vibrations are fully independent among themselves and between axis.

Hypothesis of independence of vibrations does not reduce the generality of the solution but means that information (coupling) may not be used.

As described in [5], vibrations can be precisely modeled through discrete Auto-Regressive models of order 2 (AR2), so that for a vibration *v* of central frequency *f* and damping coefficient *K* (related to the vibration Full Width at Half Max (FWHM)), we obtain:

$$v_{n+1} = a_1 v_n + a_2 v_{n-1} + b_n, \tag{1}$$

where $a_1 = 2\exp(-2\pi KfT)\cos(2\pi fT\sqrt{1-K^2}), a_2 = -\exp(-4\pi KfT)$ , *T* standing for the sampling period and $b_n$ is a generation noise which variance $\sigma_b^2$ can be related to the vibration energy.

In a similar way, we will use AR2 models for turbulent components, as they prove to be easily identified from experimental data and provide an increased performance compared to AR1 models [15, 16].

As a consequence we define a global state vector $X_n$ so that:

$$X_n = \begin{pmatrix} x_n^{tur} \\ x_{n-1}^{tur} \\ x_n^{vib,1} \\ x_{n-1}^{vib,1} \\ \vdots \\ \vdots \\ x_n^{vib,10} \\ x_{n-1}^{vib,10} \end{pmatrix}, \tag{2}$$

in which $x_k^{tur}$ ($k \in \{n, n-1\}$) is a 2 component vector accounting for turbulent angle of arrival on x and y axis, and each $x_k^{vib,i}$ ($k \in \{n, n-1\}$ and $i \in \{1,...,10\}$) is a 2 component vector accounting for vibration *i* of angle of arrival on x and y axis (vibration being different between axis).

The associated state-space model is thus defined by:

$$X_n = AX_{n-1} + \upsilon_n, \tag{3}$$

where matrix *A* is given by:

$$A = \begin{bmatrix} a_1^{tur} & a_2^{tur} & 0 & 0 & \cdots & 0 & 0 \\ I & 0 & 0 & 0 & \cdots & 0 & 0 \\ 0 & 0 & a_1^{vib,1} & a_2^{vib,1} & \cdots & 0 & 0 \\ 0 & 0 & I & 0 & \cdots & 0 & 0 \\ \vdots & \vdots & \vdots & \vdots & \ddots & \vdots & \vdots \\ 0 & 0 & 0 & 0 & \cdots & a_1^{vib,10} & a_2^{vib,10} \\ 0 & 0 & 0 & 0 & \cdots & I & 0 \end{bmatrix}. \tag{4}$$

$I$ is a 2x2 identity matrix, $a_i^{tur}, a_i^{vib,j}$ are 2x2 matrices gathering the AR2 coefficients for turbulence and vibrations state space models for x and y axis. Matrix A is thus a very sparse matrix of size 44x44. $\upsilon_n$ is a generation noise vector gathering the various noises for the various components (turbulence, vibrations). Its covariance matrix is denoted by $\Sigma_v$.

The observation (or measurement) equation of the system can be written as:

$$y_n = s_{//,n} = CX_n + PD_{ITTM}\, u_{n-2}^{ITTM} + w_n, \tag{5}$$

where:

$$C = \begin{bmatrix} 0 & I & 0 & I & \cdots & 0 & I \end{bmatrix}. \tag{6}$$

$w_n$ is the measurement noise of covariance matrix $\Sigma_w$ (2x2 matrix).

Then the LQG control equations in prediction form are given by:

$$\hat{X}_{n+1/n} = A\hat{X}_{n/n-1} + L_\infty \left( s_{//,n} - \left( C\hat{X}_{n/n-1} + PD_{ITTM}\, u_{n-2}^{ITTM} \right) \right) \tag{7}$$

$$v_n^{ITTM} = K\hat{X}_{n+1/n} \tag{8}$$

$$u_n^{ITTM} = \bar{v}_n^{ITTM} \tag{9}$$

where $K = \begin{bmatrix} -(PD_{ITTM})^{-1} & 0 & -(PD_{ITTM})^{-1} & 0 & \ldots & -(PD_{ITTM})^{-1} & 0 \end{bmatrix}$, $v_n^{ITTM}$ is an intermediate value, the newly computed voltage vector to be applied to ITTM is $u_n^{ITTM}$ a clipped version of $v_n^{ITTM}$. This is the clipped and actually applied voltage vector $u_n^{ITTM}$ that is used in the control equations to ensure coherence. Finer handling of saturation with LQG exist [17], though considering the huge ITTM dynamic compared to WFS subaperture field of view, such a situation is unlucky in normal functioning of the system.

Classically, the matrix gain is computed as:

$$\begin{aligned} L_\infty &= AH_\infty \\ H_\infty &= \Sigma_\infty C^T (C\Sigma_\infty C^T + \Sigma_w)^{-1} \end{aligned} \tag{10}$$

$\Sigma_\infty$ being the asymptotic solution of the discrete algebraic Riccati equation:

$$\Sigma_\infty = A\Sigma_\infty A^T + \Sigma_\upsilon - A\Sigma_\infty C^T (C\Sigma_\infty C^T + \Sigma_w)^{-1} C\Sigma_\infty A^T . \quad (11)$$

As no prior model is used with LQG control (we do not assume a priori parameter values for turbulence and vibration models at loop closure), ITTM control loop cannot be closed initially with LQG. An initial loop closure with fixed gain integrator is used. Then, as identification procedure is initialized at loop closure, after 1 minute the control law is updated and switches from integrator to LQG, thanks to the real-time identification of the turbulence and vibration models.

This control switching is quiet easily implemented, as the integrator is implemented using the LQG control structure by adapting the equations (7) to (9) to integrator control. During the control switching (matrices update), state vector is initialized to zero, and ITTM control voltages ($u_{n-2}^{ITTM}$) are kept, allowing correct transition between the two control laws. Of course, as initial state is initialized to zero, a few frames are necessary to converge and obtain a fully optimized correction. This transition could be improved to ensure even higher performance with almost no transition effect (see discussion in next paragraph) but provides little gain in numerical simulation, due to the quick convergence of LQG control correction.

### 3.2 Identification procedure and control update: principle and limitations

The control law thus depends on the turbulent AR2 model as well as on the various vibrations AR2 models and on the measurement noise. Performance of the control law will significantly depend on the relevance of these models. As turbulence statistics will evolve with time as well as vibrations, simply due to the evolution of the telescope mechanical configuration, one would wish to adjust these models, based on an identification procedure.

Such an identification procedure has been proposed in [8]. It provides (using open-loop or pseudo-open loop measurements) a sequential identification of turbulent component, measurement noise and a series of vibrations, in a given spectral range. This identification procedure is based on spectrum analysis. This procedure has been used on the Canary demonstrator [7], but in that precise context, identification was done prior to closed-loop observation, using a calibration run. No regular update on the fly was performed, limiting the validity of the identified models to a limited amount of time. In SAXO, the need for constant agreement with turbulent profile as well as follow-up of vibrations spectra to ensure the highest performance possible has led to adapting this procedure to closed-loop on-line identification and modification of the control law. This approach leads to a fully autonomous adaptive control.

The strategy is the following:

- Acquire closed loop data and compute pseudo-open loop measurements computing:

$$s_{//,n}^{pol} = s_{//,n} - PD_{ITTM} u_{n-2}^{ITTM} . \quad (12)$$

  In the SAXO case, the last 20000 measurements are acquired and processed.

- Apply the identification procedure described in [8].
- Compute the new control matrices. This implies update of matrices *A*, $\Sigma_\upsilon$, $\Sigma_w$ and recomputation of $L_\infty$.
- Modify in less than one frame the various matrices.

The overall procedure is repeated every minute (72000 frames).

This procedure requires some comments. First, choice of the update rate and number of accumulated data is the result of trade-offs between follow-up of turbulence and vibrations evolution and computational cost, considering that other on-line optimizations are also performed in parallel (OMGI for instance). Number of accumulated data must be high enough to provide sufficient precision in the spectral analysis but also ensure that data acquired and processed are still relevant when matrices are modified. These parameters are still to be adjusted on-sky but it has been fixed so far to a minute update rate, with 20000 acquired data cumulated.

Then, it appears that direct modification of control matrices in less than one frame is not enough. It is important to understand that, at each update of the control matrices, situation is similar as applying a new LQG control law, not

related to the previous one, except for its initial state vector which is the last estimated state with the previous control law (equivalently set of control matrices) through update of equation (7).

In the present situation, the structure of the initial state may be strongly different from one initialization to another due to the absence of ordering memory in the identification procedure. Indeed, from one identification to the next, vibrations may be identified in any order, only depending on their relative energy and on the best fit obtained by the identification procedure. A given vibration, ordered 1 at identification *n* may be ordered 3 at identification *n+1*. The result is that Kalman gains (in matrix $L_\infty$) will change and be re-ordered between identification *n* and *n+1*. The state vector will not be re-ordered accordingly (there is no way to follow-up the vibrations and their order as some may appear or disappear along the time). As a consequence, the initial state (i.e. the last estimate before control matrices update) may be affected by strong gains at the wrong place, leading to possible important and quick transitions in ITTM controls and of WFS spots. Due to the finite dynamics of ITTM and WFS, this may degrade the performance.

As a consequence, transition is smoothed by resetting to zero all the vibrations related components of the state vector at control matrices update (as turbulent angle of arrival is not concerned by this issue). This solution is clearly sub-optimal and leads to re-estimating from scratch vibrations at each control matrices update. In lab and on-sky acquisitions have proved that convergence is quick enough (few tens of frames) to avoid any significant impact on the performance.

This limitation could however be easily worked around providing some RTC modifications. It would be quite easy to implement a control law switching. In other words, as soon as new matrices are available, computation with the new control law can be started, using the same pseudo-open loop inputs but without computing the control voltages. Only the Kalman filter is used for estimation and prediction without state feedback. State vector can be fully initialized to null vector. In the meantime, the older control law is still applied in closed-loop. After some time of convergence, the two control laws (with their state vector) are switched. This solution has been tested numerically and proved to provide no significant improvement in performance. Results of this simulation are beyond the scope of this paper and shall be discussed in a dedicated article. Still, it proves that present solution of brute force zeroing of vibrations components is both easily implemented (no significant modification of RTC) and provides good performance compared to more sophisticated solution.

Finally, identification is based on pseudo-open loop measurements. This clearly relies on the hypothesis that the system is well modeled. In the SAXO case, this hypothesis is jeopardized either due to components limitations or particular use case. Indeed, first limitation is the ITTM itself. Our LQG control design assumes an infinite bandwidth component which is obviously optimistic. This has a major impact on high frequency vibration estimation and filtering, as phase lag and even component internal vibrations may affect the performance. As a work-around, vibrations filtering was initially limited to an upper frequency of 400Hz, considering the ITTM specifications (-5° phase lag at 80Hz, 1KHz -3dB bandwidth). However, actual component exhibits weaker performance than expected with reduced bandwidth (-3dB cut-off frequency of 820Hz) and extra phase lag (-15° at 80Hz with a quick increase to more than -60° at 400Hz, while this value should have been expected at 1KHz). Extra phase lag is a clear limitation in vibration estimation, considering that this phase lag is not accounted for in the control solution and will induce incorrect phasing between input vibration and correction. As a consequence, vibration estimation has been limited to an upper limit of 200Hz. Second limitation occurs in very low signal regime. Indeed, the high performance of SPHERE allowed pushing further the magnitude limit. A 300Hz sampling frequency mode has been designed to reach limit magnitude as high as 15% SR in H band for mag = 15.5 [3]. As a drawback, in this mode, global delay comes down to 1.4 leading to a clear model error both in computation of pseudo-open loop data and in the LQG control which assumes a 2 frame delay. Performance in turbulence correction is weakly affected due to the slow evolution of turbulence. As for vibrations filtering this is clearly a show stopper, leading to improper correction and even instabilities (similar phenomenon as phase lag). As a result, in this mode, vibration filtering is shut down at the LQG control level (corresponding parts of matrices set to zero). This is a clear limitation that could be easily corrected accounting for global delay in the pseudo-open loop data computation and in the control law as discussed in [18] for instance.

## 4. LQG CONTROL IN LAB: VALIDATION AND PERFORMANCE

We discuss in this section validation and performance of LQG on SAXO as obtained during AIT. We first discuss experimental conditions, then focus on identification procedure and LQG performance.

### 4.1 Experimental set-up and tests conditions

In the following, tests have been performed at Grenoble, with the full SPHERE system working at 1.2KHz without EMCCD gain on WFS. Input turbulence is generated by the turbulence simulator, placed upstream from SPHERE entrance focal plane. The turbulence is generated thanks to 2 rotating Kolmogorov phase screens. In the present situation turbulence seeing is 0,85" (nominal conditions), average wind speed is 10m/s and flux conditions are equivalent to high flux. In addition to turbulence, local vibrations can clearly be detected. These vibrations are 19.8Hz, 45Hz and 77Hz mainly. They are quite stable in time. Of course, some vibrations can evolve and local turbulence may induce not reproducible effects. Nevertheless, long ranges acquisitions have shown that input signal is stable enough for relevant comparison even if tests of control laws are obviously performed sequentially thus at different moments. Figure 2 shows a typical Power Spectrum Density (PSD) of the open-loop WFS measurement projected onto the $(s_1, s_2)$ basis (i.e. the angle of arrival). Here the projection onto $s_1$ mode (considered as x axis) is proposed. A high energy low frequency can be detected around 0.1Hz which is due to residual wobble of the phase screen.

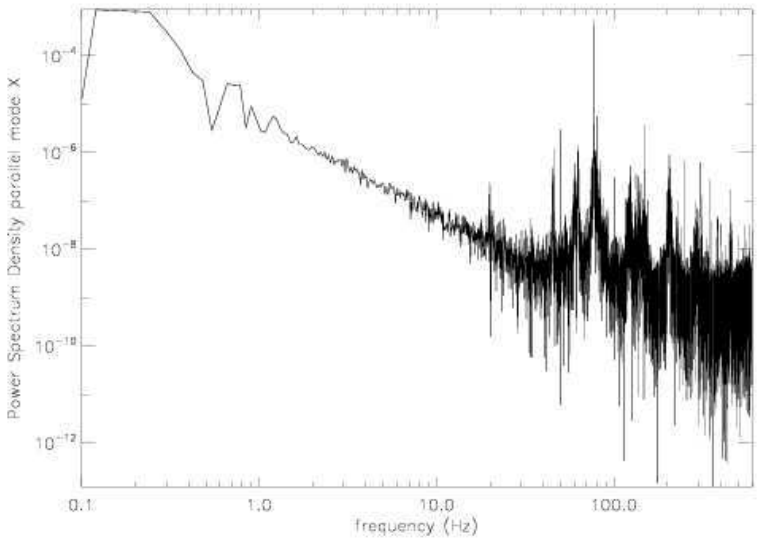


Figure 2: Open-loop power spectrum density of WFS measurement projected onto $S_1$ mode (angle of arrival along x axis, here arbitrary unit), turbulence as well as local vibrations are clearly visible.

In the following, we shall compare integrator performance and LQG performance, with on-line regular identification. Gain of integrator has been optimized per axis for correct comparison to a 0.5 gain. Concerning LQG, turbulence and vibrations are corrected, and on-line identification and control law update is regularly performed on a per minute basis. As explained in previous section LQG is first initialized as a fixed gain integrator before first identification and control matrices update. This first step is of course discarded in performance comparison as we focus on the steady state regime. To ensure correct estimation of performance of each control law, performance is estimated over various rotations of the phase screen.

### 4.2 Identification and LQG performance

Figure 3 shows closed-loop PSD of WFS measurement on $(s_1, s_2)$ modes (noted hereafter residual angle of arrival in x and y axis), either using integrator (black) or LQG (red). Clear reduction of vibrations, in particular the 77Hz vibration, is visible. The gain in performance is even more visible on the cumulated PSD of the same signals, proposed in Figure 4.

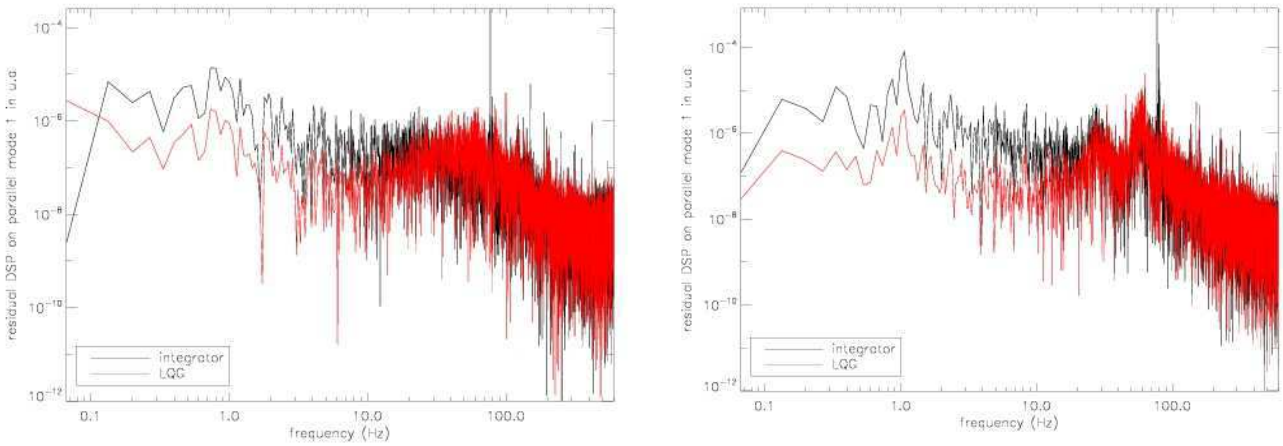


Figure 3: PSD of residuals of angle of arrival, either using integrator (black) or LQG (red) (left: x axis, right: y axis).

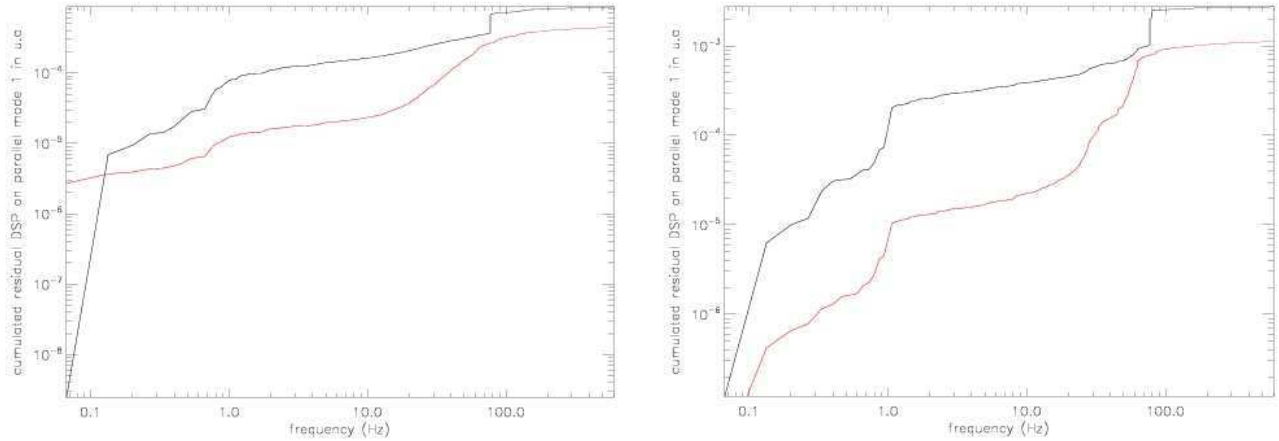


Figure 4: cumulated PSD of residuals of angle of arrival, either using integrator (black) or LQG (red) (left: x axis, right: y axis). Turbulence conditions are 0.85" seeing, 10m/s.

Clear attenuation of the 77Hz vibration is detected by absence of the related step in cumulated PSD for LQG. In these tests, the other vibrations (45Hz for instance) are of negligible energy and thus not detected.

One can also note a better rejection of low frequency turbulent component, on a broader spectral range, due to LQG accounting for turbulence temporal characteristics: instead of the classic integrator 20dB/decade rejection, with infinite rejection at 0Hz, LQG exhibits a finite rejection at 0Hz, but provides a rejection of input signal adapted to its spectral profile.

For these tests, residual jitter in mas rms estimated on visible path was 2.7 for integrator and 1.7 for LQG, indicating a clear gain in performance, even if integrator performance was within the specification in these good conditions.

Similar test has been performed in weaker turbulence conditions (0.62", same wind speed), allowing to isolate more clearly the vibration rejection effect. Results in terms of cumulated PSD are proposed in Figure 5. This test also shows that first vibration (19.8Hz) is not filtered by LQG as the spectral bandwidth for vibration estimation and correction was set to [20, 200] Hz, but reversely vibrations out of this bandwidth have not impact on LQG behavior. Of course, this bandwidth can be modified and extended to lower frequencies.

During this test residual jitter in mas rms has been **reduced by a factor 3 using LQG compared to integrator**.

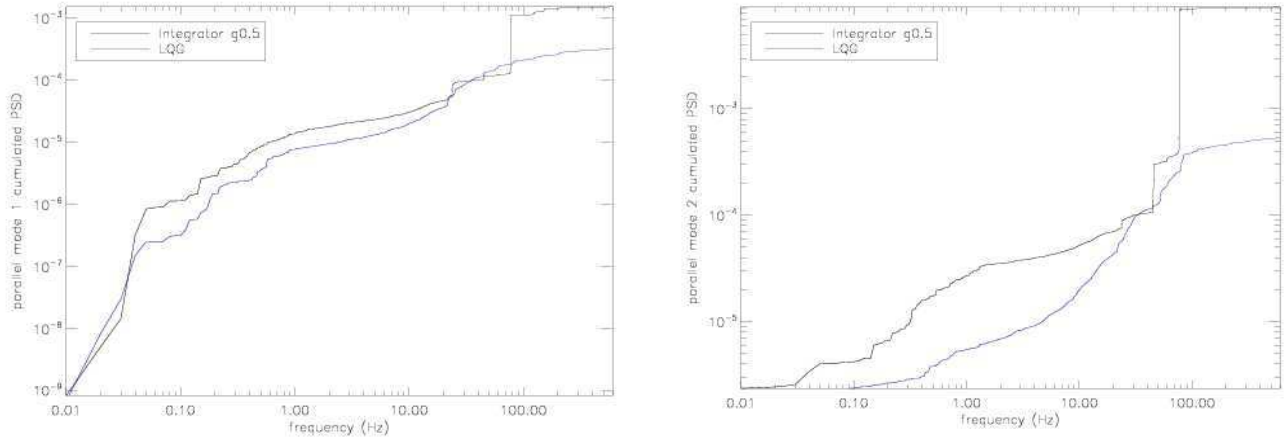


Figure 5: cumulated PSD of residuals of angle of arrival, either using integrator (black) or LQG (red) (left: x axis, right: y axis). Turbulence conditions are 0.62" seeing, 10m/s.

Considering once again the 0.85" seeing test conditions, one can evaluate stability of the LQG performance along time, while control matrices are updated. Acquisitions have been performed over 20 rotations of phase screen. Performance of LQG is stable with a mean value of 1.7 mas rms and a standard deviation of only 0.06 rms.

### 4.3 Performance in poor conditions and control tuning

Tests of SAXO in worse conditions have been performed with the full LQG control scheme (poor seeing 1.2", high wind speed up to 30m/s, very low flux equivalent to mag=15 in K). Results of these tests are discussed in [3]. These tests make use of course of the overall SAXO system, and it is difficult to extract the sole contribution of ITTM control. Still, as performance is reached both in terms of Strehl Ratio and residual jitter, they prove that:

- The ITTM control law is stable even in poor conditions
- The identification procedure is efficient and allows tuning of the ITTM control to turbulence conditions
- The global performance in residual jitter is well within (even beyond) specifications.

## 5. FIRST COMMISSIONNING ON-SKY RESULTS

SPHERE has seen its first on-sky photon the 4$^{th}$ of May and the AO loop has been closed less than 20 min after the beginning of operation. The three first weeks of May have been dedicated to functional tests and very first performance analysis. We present here the very first results obtained on-sky, knowing that, they are deduced from the very first data during the early days of the instrument commissioning. Exhaustive analysis and full performance assessment will be provided in the coming months after the various SPHERE commissioning run (from July to October 2014).

### 5.1 The input signal characteristics

Before any performance analysis, it is of much interest to focus on the turbulent input signal as seen by SPHERE. Indeed, SPHERE, with its 1.2KHz sampling frequency, offers the first high frequency characterization of turbulence on-sky with VLT, with a 40x40 Shack-Hartmann WFS. We focus here once again only on angle of arrival, though higher order modes analysis have been started and will be discussed after the various commissioning runs.

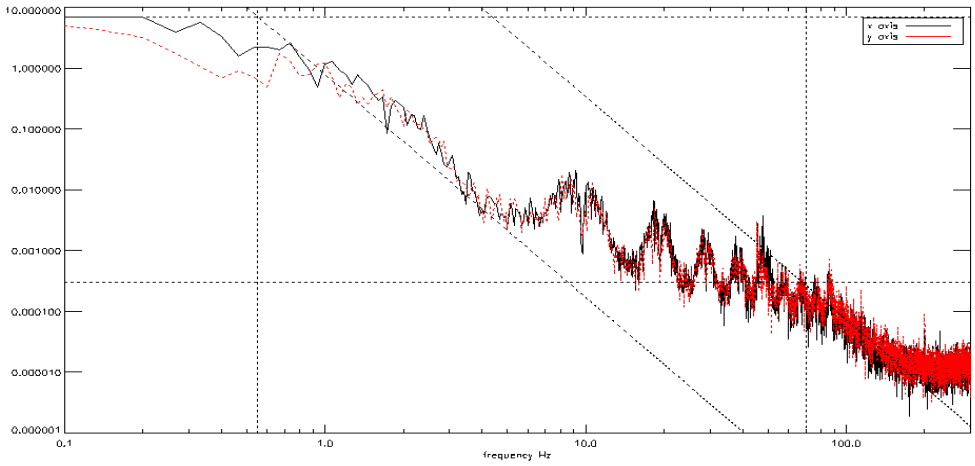


Figure 6: open-loop PSD of angle of arrival (subsampled at 600Hz) along x (black) and y (red) axis. Approximative asymptotic profiles with -11/3 power are proposed.

Figure 6 shows the temporal PSD of angle of arrival, as seen during first commissioning in open-loop on a bright target (HR5670, magnitude of 4, seeing of 0.7", wind speed estimated to 15m/s). This PSD is however obtained on sub-sampled data, by a factor 2, so limited to 300Hz. In spite of this defect, this profile presents various original features. First part of PSD profile exhibits a standard profile with somehow a horizontal asymptote at very low frequency then a -11/3 asymptotic profile. This behavior quickly changes over 10Hz with 2 different effects:

- Apparition of regularly spaced structures, similar to twin large vibrations, initially centered around 10Hz, and then regularly spaced by 10Hz approximately
- A modification of the 'natural' asymptotic -11/3 profile that can be expected with an increase of PSD between 7Hz and 70Hz approximately, beyond a -11/3 asymptotic profile appears once again.

Origin of the so-called twin vibrations and their harmonics has been quickly identified as results of UT3 mirror 2 (TM2) active control, which includes some internal filtering of vibrations. This explains the particular profile observed which is not a twin vibration but more probably the residue of filtering of a vibration by a notch filter, not large enough to filter out the foot of the vibration, with apparition of replicas. Figure 7 to 9 propose residual PSDs in similar conditions with use of standard fixed gain (g=0.4) integrator, here with full sampling, and with TM2 control set in various conditions (slow, fast and no Field Stabilization active control). The residual PSDs allow clearly distinguishing the high order contributions mentioned above (use of integrator avoids also interference with LQG filtering). Vibrations residues are clearly dependent from the TM2 active control, and disappear once it is shut down. Still, analysis of cumulated PSDs in open or closed loop, shows that contribution of these vibration residues to the overall angle of arrival is not significant. This result is corroborated by global performance: using integrator, residual jitter in mas rms on sky, with TM2 active or not is respectively of 11.1 or 10.5 (computation based on WFS real-time data).

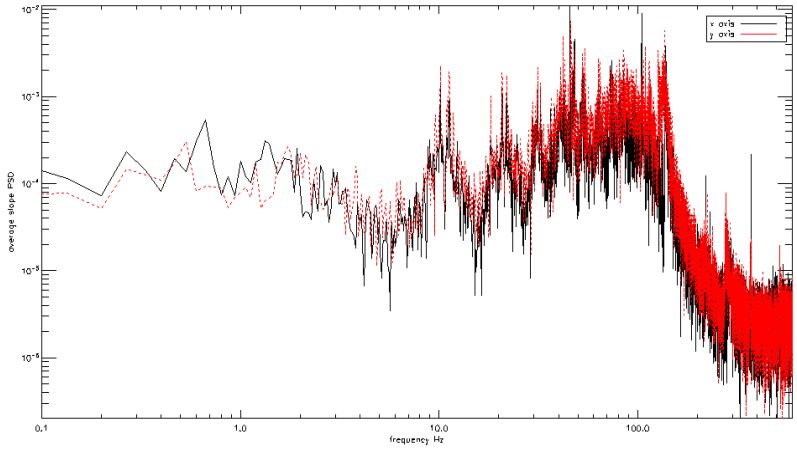


Figure 7: closed-loop PSD of residual angle of arrival along x (black) and y (red) axis, with fixed gain integrator, and slow TM2 active control.

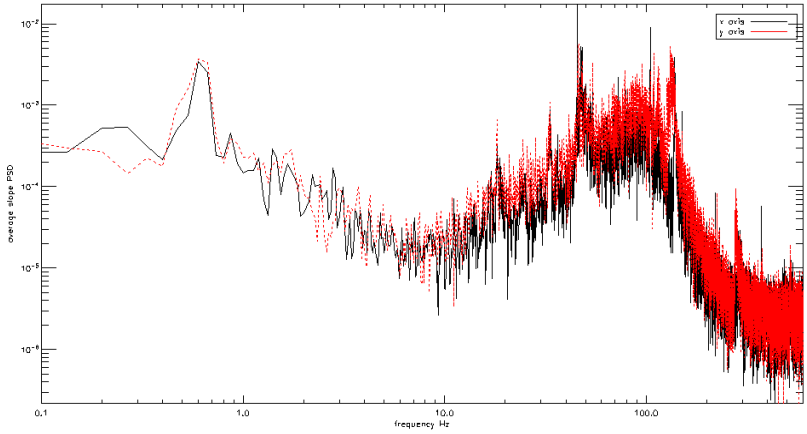


Figure 8: closed-loop PSD of residual angle of arrival along x (black) and y (red) axis, with fixed gain integrator, and fast TM2 active control.

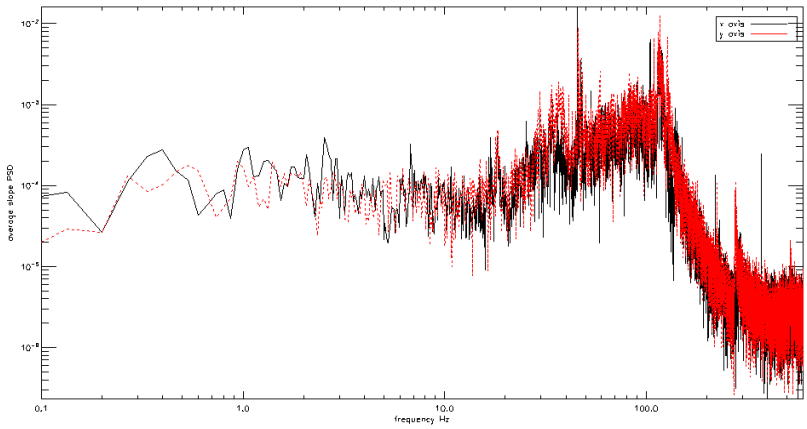


Figure 9: closed-loop PSD of residual angle of arrival along x (black) and y (red) axis, with fixed gain integrator, and no TM2 Field Stabilisation active control.

On the contrary, even with TM2 Field Stabilisation active control OFF, the residual PSD still exhibit an unnatural strong contribution between 10Hz and 100Hz approximately in comparison with the residuals obtained in lab on turbulent phase screens (Figure 3). Origin of this contribution is unknown, though it has been shown that it is not related to the control law (same issue either with LQG or integrator), nor to the SPHERE bench (absence of any contribution or significant vibrations using internal source). Turbulent contribution is unlucky at so high a frequency. This contribution appears in all open and closed loop data acquired during first commissioning.

A very first analysis of the impact of this high frequency perturbation on the system performance in term of residual jitter has been carried out. Based on the open-loop asymptotic profile proposed in Figure 6 two asymptotic profiles have been identified. First fit (fit 1) only focuses on the low frequency behavior and is considered as normal while fit 2 adds to the fit 1 an asymptotic approximation of the high frequency perturbation, leading to an abnormal profile. Corresponding fits are proposed on Figure 10. Using these asymptotic profiles and theoretical transfer function of integrator, and providing that measurement noise can be neglected in a first approximation in the current high flux conditions, one can easily estimate the relative increase of residual jitter only due to the high frequency contribution, which is in this case about a factor 5 in mas rms.

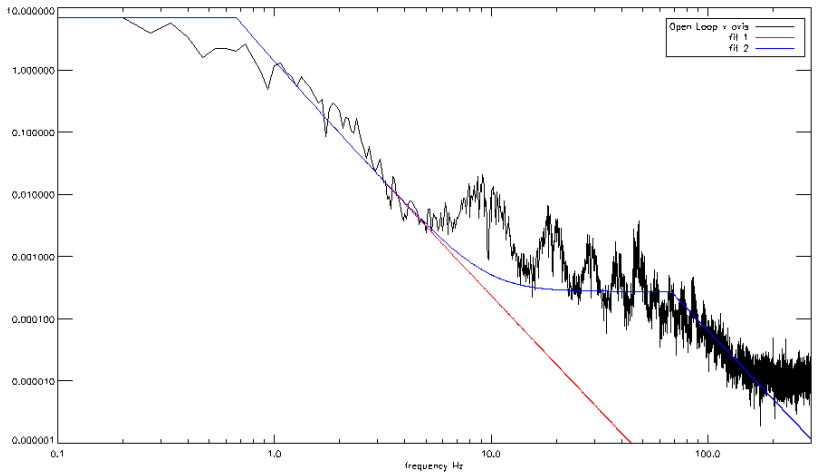


Figure 10: open-loop PSD of angle of arrival (subsampled at 600Hz) along x (black). Asymptotic profiles with -11/3 power are proposed: fit 1 only fits the lower frequency part, fit 2 accounts also for the high frequency perturbation with a composite profile.

Though it is a very preliminary and brute force analysis, it shows that this high frequency contribution can clearly affect the global performance of the system, irrespective of the vibration issue related to TM2, as well as the ITTM control solution.

### 5.2 On-sky identification

We now focus on on-sky identification of the turbulence and vibrations models as provided by the on-line identification procedure, considering the particular input signal discussed previously. These tests have been performed on a bright target (HR5670, mag=4) with medium conditions (1” seeing, average wind speed of 15m/s).

Figure 11 proposes a typical result of the identification procedure. The turbulent AR2 model as well as the 10 vibrations AR2 models of x and y axis angle of arrival as obtained during one on-line identification have been recorded and processed into composite PSD. This profile is compared to the PSD of the pseudo-open loop angle of arrival along x and y axis that has been used by the identification procedure.

As can be seen, turbulence profile is well identified, though one can note that some compromise has been found by the identification procedure between the low frequency profile (following the -11/3 asymptote) and the contribution of high frequency perturbation. Measurement noise estimation is visible in the very high frequency horizontal asymptote

between 450Hz and 600Hz with correct matching with pseudo-open loop PSD. Vibrations located between 40 and 50Hz, at 90Hz and 130Hz have been correctly identified. But vibration residues due to TM2 active control have not been identified. Detailed analysis show that these components either are below the lower limit for vibration estimation (20Hz) or are too smooth to be identified. Indeed, identification procedure orders and selects vibrations depending on their relative energy, in this case too small.

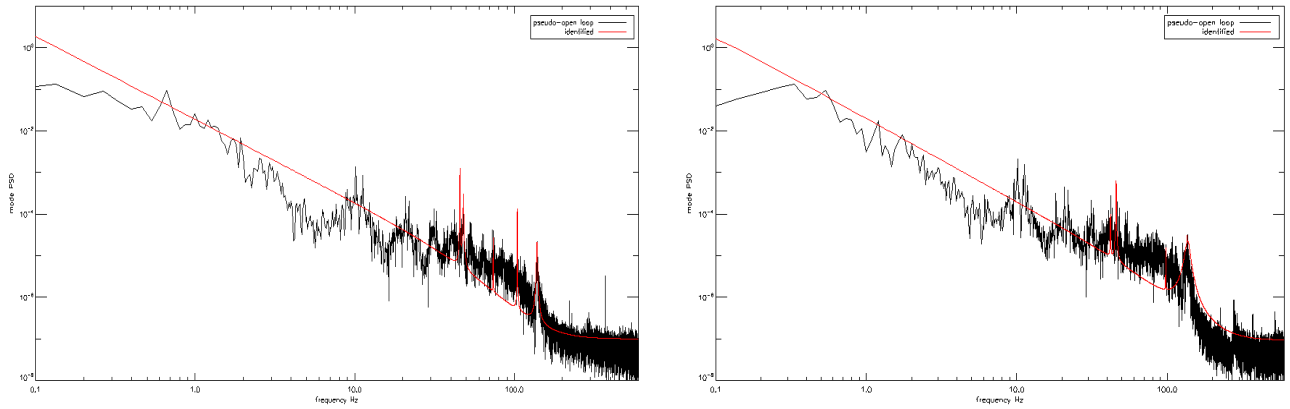


Figure 11: pseudo-open-loop PSD of angle of arrival (black) along x axis (left) and y axis (right) and result of identification procedure for each axis in terms of AR2 model for turbulence plus various identified vibrations AR2 models and measurement noise contribution.

### 5.3 LQG performance on-sky

We now address the LQG performance on-sky, combined with the on-line model identification procedure. We compare performance with standard integrator. The current conditions were better, with a 0.5" seeing and an 8m/s average wind speed. A bright target is considered (HR5249 mag=4.4). Loop has been closed either with LQG or integrator.

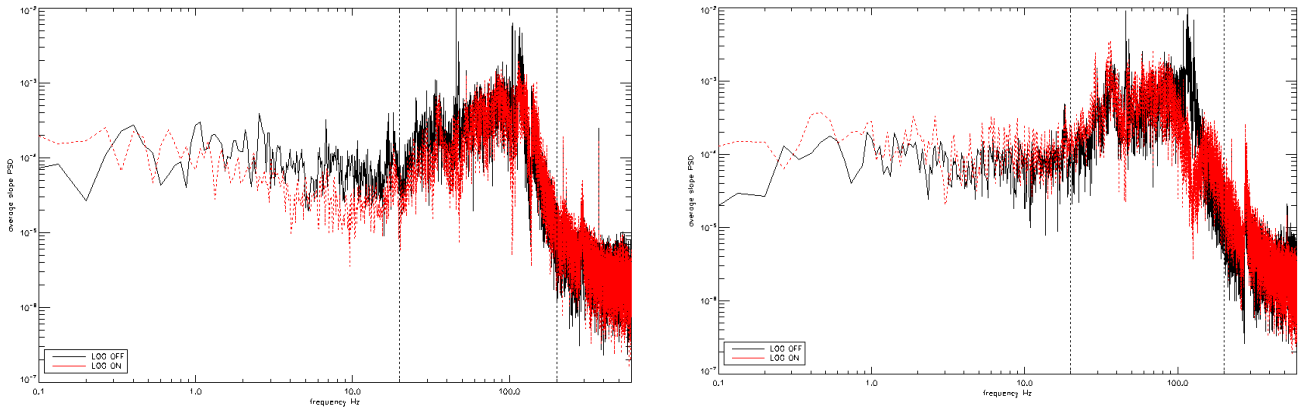


Figure 12: closed-loop PSD of residual angle of arrival along x axis (left) and y axis (right) with either integrator (black) or LQG (red). Vertical dotted lines indicate lower and upper bound for vibration identification.

Figure 12 shows PSD of the residual angle of arrival on both axis, using either control solution. As low frequency behavior is similar for both control solutions. Main difference occurs between 20 and 200Hz due to vibrations filtering. On both axis the 45Hz vibration is clearly suppressed. Then various components are filtered on each axis between 100 and 130Hz. This is confirmed on the cumulated PSD proposed in Figure 13 through reduction of the steps introduced on the cumulated PSD at these frequencies.

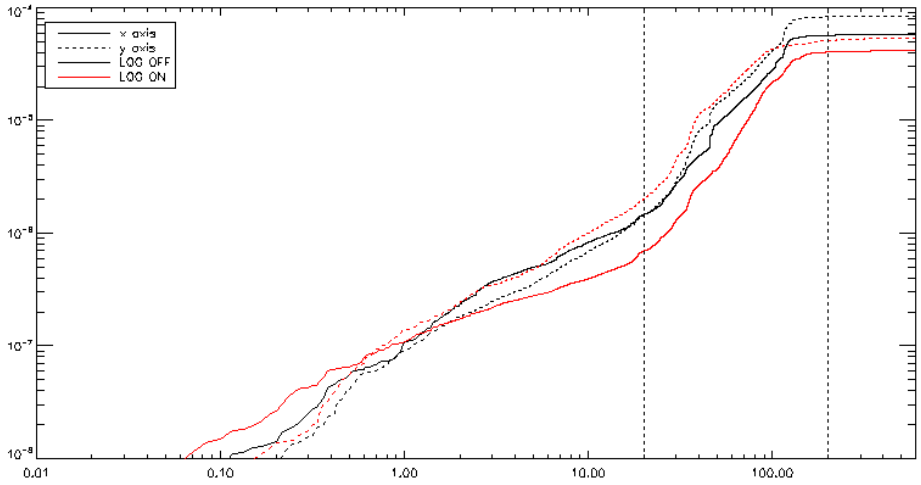


Figure 13: closed-loop cumulated PSD of residual angle of arrival along x axis (solid line) and y axis (dotted line) with either integrator (black) or LQG (red). Vertical dotted lines indicate lower and upper bound for vibration identification.

In term of global performance, residual jitter is 11 mas rms with integrator and reduced to 9 mas rms with LQG. While these figures clearly underline the gain brought by LQG, they are both well beyond the specification of 3 mas rms. But as discussed in Section 5.1 this performance degradation could probably be related to the high frequency perturbation, clearly visible on the residual PSD (see previous section).

## 6. CONCLUSION

SPHERE and its XAO system are currently in commissioning. In lab experiments have demonstrated the performance, the reliability and the stability of the AO loops (and of SAXO and SPHERE as a whole), in spite of some limitations such as the High Order DM [3]. The ITTM control loop in particular implements the first on-sky LQG control for an operational system, coupled with on-line identification of turbulence and vibrations models, leading to propose a fully auto-tuned optimal control. This unprecedented control scheme in AO has demonstrated its performance in lab with a clear gain in performance compared with standard integrator control, basically due to vibration filtering. Some limitations have also been identified, due to ITTM component itself (limited bandwidth, extra phase lag), or to the functioning at slower frame rate for faint targets leading to an unexpected non integer frame delay, or also to transition issues at control law updates. Last issue has been addressed, though with a very straightforward solution, but that ensures stability. A more astute solution, based on control switching has been tested, though not discussed here and proved to bring no significant gain in performance. These limitations have so far led to some restrictions in use of LQG control or identification procedure, though solutions to overcome these limitations already exist, but require significant modifications of the RTC software.

The first on-sky commissioning has confirmed laboratory tests by providing unprecedented images and coronagraphic data on the VLT [2,3]. The system stability has been re-demonstrated on-sky and the first performance assessment is more than encouraging. Residual jitter is stronger than expected (Strehl Ratio lower). In addition to bad weather conditions, we have shown that residual vibrations on the telescope M2 but also other high frequency perturbations could greatly explain this loss of performance, whatever the control law. Now some additional tests and investigations are required to understand these effects. In addition, fine tuning of the system as well as control parameters should provide more consolidated performance and stability assessment and allow reaching, in the coming months, the full system performance.

## ACKNOWLEDGEMENT

The work was partly funded by the European Commission under FP7 Grant Agreement No. 312430 Optical Infrared Coordination Network for Astronomy and by the Office National d'Etudes et de Recherches Arospatiales (ONERA) (in the framework of the NAIADE Research Project)

## REFERENCES

[1] J-L. Beuzit, *et al*, "A planet finder instrument for the VLT," in *Proceedings of IAU Colloquium 200, Direct Imaging of Exoplanets: Science & Techniques* (Cambridge University Press, 2005), pp. 317–323
[2] J.-L. Beuzit *et al*, "SPHERE: a planet finder instrument for the VLT", paper **9148-17,** this proceeding
[3] T. Fusco *et al*, "Final performance and lesson-learned of SAXO, the VLT-SPHERE extreme AO, from early design to on-sky results", paper ,this proceeding
[4] J.-F. Sauvage *et al*, "Wave-front sensor strategies for SPHERE: first on-sky results and future improvements", paper 9148-155, this proceeding
[5] C. Petit *et al*, "First laboratory validation of vibration filtering with LQG control law for adaptive optics," Opt. Express 16, 87–97 (2008)
[6] J. Lozi *et al*," Current results of the PERSEE testbench: the cophasing control and the polychromatic null rate", SPIE Optical Engineering+Applications Proc., pp 81510B-81510B-17, 2011
[7] G. Sivo *et al*, "First on-sky SCAO validation of full LQG control with vibration mitigation on the CANARY pathfinder". Optics Express, in revision 2013
[8] S. Meimon *et al*, "Tip–tilt disturbance model identification for Kalman-based control scheme: application to XAO and ELT systems," J. Opt. Soc. Am. A 27, 122–132 (2010)
[9] C. Petit *et al*, "Optimisation of the control laws for the SPHERE XAO system," in "Proc. SPIE," (2008), pp. 70151D– 12
[10] T. Fusco *et al*, "Closed-loop experimental validation of the spatially filtered Shack-Hartmann concept", Optics Letters, Vol. 30, Issue 11, pp. 1255-1257 (2005)
[11] E. Fedrigo, R. Donaldson, "SPARTA: the ESO standard platform for adaptive optics real time applications", Proc. SPIE 6272, (2006)
[12] J-F Sauvage *et al*, "Calibration and Pre-Compensation of Non-Common Path Aberrations for eXtreme Adaptive Optics", JOSA A, Vol. 24, Issue 8, pp. 2334-2346 (2007)
[13] E. Gendron and P. Léna, "Astronomical adaptive optics i. modal control optimization", Astronomy and Astrophysics 291, pp. 337-347, 1994
[14] C. Kulcsár *et al*, "Optimal control, observers and integrators in adaptive optics," Opt. Express 14, 7464–7476 (2006).
[15] Le Roux *et al*, "Optimal control law for classical and multiconjugate adaptive optics," J. Opt. Soc. Am. A 21, 1261–1276 (2004).
[16] C. Petit *et al*, "LQG control for adaptive optics and multiconjugate adaptive optics: experimental and numerical analysis," J. Opt. Soc. Am. A 26, 1307–1325 (2009).
[17] C. Kulcsár *et al*, "Can LQG adaptive optics control cope with actuator saturation ?" in "Adaptive Optics: Analysis and Methods/Computational Optical Sensing and Imaging/Information Photonics/Signal Recovery and Synthesis Topical Meetings," (Optical Society of America, 2007), p. PMA1.
[18] H.-F. Raynaud *et al*, "Minimum-variance control of astronomical adaptive optics systems with actuator dynamics under synchronous and asynchronous sampling", International Journal of Robust and Nonlinear Control, 21(7):768–789, 2011, on line in May 2010.